The effects of moist entropy and moisture budgets on tropical cyclone development

Ana Juračić,[1] and David J. Raymond,[1]

Corresponding author: Ana Juračić, Department of Physics and Geophysical Research Center, New Mexico Institute of Mining and Technology, Socorro, New Mexico, USA (ana.juracic@gmail.com)

[1]Department of Physics and Geophysical Research Center, New Mexico Institute of Mining and Technology, Socorro, New Mexico, USA

Key Points.

- Moist entropy budget can possibly be used to differentiate between intensifying and non-intensifying tropical cyclones
- Moisture tendency relates to current intensity of a tropical cyclone, with higher values for stronger tropical cyclones

Abstract. This paper examines the moist entropy and moisture budgets in tropical cyclones, as well as their relation to tropical cyclone's development. This analysis focuses on the dropsonde data collected during Hurricane and Severe Storm Sentinel (HS3) project and the accompanying satellite data. Two tropical cyclones of interest are Tropical Storm Gabrielle (2013) and Hurricane Edouard (2014). There were three research flights into Gabrielle (2013), during its non-developing and decaying stages. Edouard (2014) was visited four times in different stages of its life-cycle, twice during the intensification and twice during the decay. Also, we extended our analysis on the larger dataset, consisting of 11 non-intensifying and 12 intensifying systems. Our study shows that the moist entropy tends to increase during intensification and decrease during non-intensifying stages. On the other hand, the moisture budget relates better to the tropical cyclone's current intensity than its development. The sign of the moist entropy tendency depends on the ability of surface fluxes and irreversible moist entropy generation to overcome lateral export of moist entropy and loss due to radiative cooling. Edouard's decay during the last research flight was likely the result of increasing wind shear and low sea surface temperatures. During its decay, Gabrielle had strong column-integrated lateral export of moist entropy and drying between 1 and

4 km height. This is probably the consequence of a dry environment at multiple levels, amplified by a warm and dry anomaly left behind by previous convective activity.

1. Introduction

In a tropical cyclone's evolution, both dynamics and thermodynamics play an important role. They affect each other and make the environment either hostile or conducive for tropical cyclone development; they can make the storm itself stronger or weaker [*Emanuel*, 1999; *Emanuel et al.*, 2004; *Gjorgjievska and Raymond*, 2014; *Raymond et al.*, 2014]. The interactions between the tropical system and the environment, as well as between the winds and the thermodynamic variables can be hard to capture, especially in observational data. With new field programs and growing availability of good in situ data this puzzle may become easier to solve. Dropsonde data prove to be one of the most useful in situ data sets. They provide very good vertical resolution and good horizontal coverage for in-storm or storm-environment interaction analysis, depending on the area of coverage.

This paper will address how moist entropy and moisture budgets affect a tropical cyclone's development. If we can determine certain patterns in those budgets that relate to intensification or decay, those budgets could be another useful tool in forecasting the intensity of tropical cyclones. The terms that contribute to the entropy budget are surface fluxes, lateral import or export of moist entropy, radiative cooling, and irreversible generation of moist entropy. The moisture budget consists of surface fluxes, lateral import of moisture and rainfall. For our analysis, we use the dropsonde data from National Aeronautics and Space Administration's (NASA's) Hurricane and Severe Storm Sentinel (HS3) project [*Hock et al.*, 2016]. This project focused on processes during hurricane formation and intensity change in the Atlantic Ocean. Because of great horizontal and vertical range provided by the NASA's unmanned aerial vehicle Global Hawk, HS3 research flights could

target both storm-scale and large-scale processes, which provides a good setup for storm-environment interaction analysis. Two storms are chosen for case studies: Gabrielle in 2013 and Edouard in 2014. Gabrielle decayed or did not develop during the three research flights, so it will be used as an example of a non-intensifying storm. Edouard, on the other hand, developed into a Category 3 hurricane and four research flights collected dropsonde data during intensification and decaying stages, creating a suitable data set for analysis of a tropical cyclone's life-cycle. Even though this is not the first effort to estimate the relationships between the thermodynamic budgets and tropical cyclone evolution, this paper's strength lies in the analysis using the combination of dropsonde and satellite data. According to our literature review, this is the first attempt of estimating the entire moist entropy budget in a tropical cyclone from the observational data.

The budgets of dynamic and thermodynamic variables are used in many papers to explain the development of tropical systems. Some authors explore the entropy budget of moist convection by viewing the water vapor transport as an imperfect heat engine [*Pauluis and Held*, 2002a, b; *Pauluis*, 2011; *Warner*, 2005]. These papers show in detail the magnitudes of irreversible generation, surface fluxes, and the radiative loss of entropy in the model, during the moist convection. There is one more part of the budget that is not present in their model setup. It is the divergence of entropy flux, or the lateral entrainment of moist entropy, which comes from the interaction with the environment.

Neelin and Held [1987] introduced the gross moist stability (GMS), a parameter related to the convection strength. It depends on the net outflow of moist static energy. Minima in GMS correspond to tropical convergence zones. An alternative approach to the calculation of GMS is to use moist entropy instead of moist static energy. Those two variables

are closely connected and both are quasi-conserved in moist processes. *Raymond et al.* [2007] modified the calculation of GMS by normalizing the net lateral export of moist entropy by lateral import of moisture. This normalized gross moist stability (NGMS), in conjunction with the net change in moist entropy, can be directly used to calculate the net rainfall rate in the steady state. The net precipitation is inversely proportional to NGMS, meaning that smaller positive NGMS leads to more precipitation [*Raymond et al.*, 2007]. Negative NGMS results in a positive feedback effect, further drying out the dry and further moistening the moist environments [*Sessions et al.*, 2010]. The latter case indicates that lateral import of moist entropy in conjunction with lateral import of moisture would increase the possibility for intensification. *Raymond and Sessions* [2007] used a cloud resolving model to examine the environmental moistening and stabilization effects on NGMS and rainfall. Their results show the increase of rainfall and decrease of NGMS for moister or more stable environments. They related such behavior to a more bottom-heavy vertical mass flux, which decreases the depth of the inflow layer, inhibiting the import of low entropy mid-level air. The composite analysis from *Masunaga and L'Ecuyer* [2014] shows that the onset of deep convection happens when moist static energy (MSE) divergence and GMS reach values close to zero. Deep convection keeps GMS small, but positive, by strong export at upper levels. In their analysis, this is followed by increase in MSE divergence, due to stratiform rain occurring in mature convective systems. *Inoue and Back* [2015] explore MSE budgets and NGMS on different time scales. They show that horizontal NGMS varies more and has smaller values than the vertical component. The studies done so far [*Raymond et al.*, 2007; *Raymond and Sessions*, 2007; *Raymond et al.*, 2011; *Masunaga and L'Ecuyer*, 2014] show that the smaller the (N)GMS and the

lateral moist entropy export, the higher the chance for a system's development. This is likely due to the greater precipitation rate and associated heating per unit surface moist entropy flux. In the steady state this flux is correlated with lateral entropy export.

A lot of effort has been made to explain cyclogenesis using the vorticity and moist entropy budgets [*Raymond and López Carrillo*, 2011; *Raymond et al.*, 2011; *Gjorgjievska and Raymond*, 2014]. *Raymond and López Carrillo* [2011] attributed the rapid spin-up of Pacific tropical cyclone Nuri to strong vorticity convergence in the planetary boundary layer. That convergence was a response to the strong low-level increase with height of the vertical mass flux. *Raymond et al.* [2011] found that in addition to low level convergence of vorticity, the bottom heavy vertical mass flux profile also reduces the lateral export of moist entropy per unit mass. Even though these papers focused on cyclogenesis, they do touch on the effect those budgets have on further tropical cyclone development, even to the hurricane stage. However, none of those analyze in detail what happens when a tropical storm or a hurricane decays and what role the moist entropy and moisture budgets play then. *Raymond and López Carrillo* [2011] also found that Nuri was protected from the environmental intrusion by having closed circulations that overlap in the planetary boundary layer and at 5 km. This is similar to the hypothesis by *Dunkerton et al.* [2009] where the development occurs due to existence of a protected region, where the storm-relative winds and the dry air intrusion are weak.

We will test the hypothesis that moist entropy increase within a tropical cyclone, a net result after considering all parts of the budget, supports intensification. The effects of moisture and moist entropy budgets in different stages of tropical cyclone's life-cycle and possible causes for the decay of Gabrielle and Edouard will be discussed as well. Section

115 2 of this paper explains the data and methods used for the analysis. Case studies are
116 explained in Section 3. Results are in section 4, while conclusions are in section 5.

2. Data and Methods

2.1. HS3 project

117 The dropsonde data used in this analysis were collected during NASA's Hurricane and
118 Severe Storm Sentinel (HS3) project [*Hock et al.*, 2016]. The field measurements were
119 done during the peaks of three hurricane seasons in the Atlantic, late August through
120 early October, in 2012, 2013, and 2014. The base of operations was NASA Wallops Flight
121 Facility at Wallops Island, Virginia. The research flights with dropsondes were conducted
122 with the NASA Global Hawk 872 (AV-6) unmanned aircraft. This allowed the dropsonde
123 data to reach altitudes of 18-20 km. Also, Global Hawk flights have greater range and
124 spatial coverage than flights with manned aircraft. The storms could be targeted further
125 to the east than usual, just a couple of days after emerging from the African coast.
126 The number of dropsondes per flight varied between 50 and 88. The spatial coverage
127 is on the order of $10^\circ \times 10^\circ$ and the time between the first and the last drop may be
128 over 12 hours. The unique Global Hawk capabilities allowed for HS3 research flights to
129 have unprecedented spatial and temporal dropsonde sampling by a single aircraft. The
130 objective of the project was to target both the inner core and environmental scale, so
131 the general flight pattern was a lawnmower pattern, followed by center crossings. The
132 lawnmower part allows for the sampling of both the environment and the tropical cyclone
133 inner core. The changes to this general flight pattern depended on the synoptic situation
134 and the position of the tropical cyclone. There was enough dropsonde coverage to examine

the storm-environment interaction in all missions used in this analysis. The peculiarities of each research flight will be discussed in more detail in the case studies section.

2.2. Methods

All dropsonde data from the HS3 project were quality controlled by the Earth Observing Laboratory at the National Center for Atmospheric Research (NCAR) [*Young et al.*, 2013; *UCAR/NCAR - Earth Observing Laboratory*, 1993-present]. The quality controlled dropsonde data were further manually inspected for missing or unrealistic data, and linearly interpolated to a vertical resolution of 25 m. This data set was then analyzed with an analysis tool called 3D-Var, described in *López Carrillo and Raymond* [2011]. This tool takes spatially nonuniform dropsonde data and interpolates it on a regular grid. For the purpose of this analysis, the horizontal grid resolution is 0.5° with vertical levels every 200 m from the surface to an altitude of 16 km. The horizontal domain depends on the dropsonde coverage and the size of the system at the time of the research mission. 3D-Var enforces mass continuity when interpolating horizontal wind speeds and calculating vertical velocity. It also uses the storm co-moving reference frame, with the storm speed calculated from Best Track data.

The analysis is concentrated on the storm itself by creating a smaller domain, or mask, centered on the storm center during the research flight. The storm center is detected manually from the vorticity field at an altitude of 2-3 km. The domain is kept within the dropsonde coverage, to avoid extrapolation. The mask dimensions are $4° \times 4°$ for all cases studied here. This size captures most of the vorticity signal for all missions, while being limited to the system's immediate environment. It is not clear what size of mask would be the best choice in general, since tropical systems' sizes can vary greatly,

not just among themselves, but also with time. We opted for a universal size instead of encompassing the specific characteristics, since it is hard to establish the precise position of the storm-environment interface. A universal size is less subjective and the HS3 dropsonde distribution is large enough to accommodate such choice.

The 3D-Var analysis outputs the measured data, such as pressure, temperature, relative humidity and wind speeds, on the regular grid of our choosing. From those fields, other dynamic and thermodynamic variables, such as moist entropy, mixing ratio of water vapor, and vorticity, are calculated. Furthermore, by combining these variables with wind fields, it is possible to calculate tendencies due to lateral import, or lateral entrainment. Moisture lateral entrainment, at each grid point, is calculated as follows:

$$LEM = -\nabla_{\mathbf{h}} \cdot (\rho \mathbf{v_h} r) \tag{1}$$

ρ is the air density, $\nabla_{\mathbf{h}}$ is the horizontal differential operator, $\mathbf{v_h}$ is the storm-relative horizontal wind velocity and r is the mixing ratio of water vapor. The calculation of moist entropy lateral entrainment is similar:

$$LEE = -\nabla_{\mathbf{h}} \cdot (\rho \mathbf{v_h} (s - s_0)) \tag{2}$$

In this equation, everything is as in equation (1), with s and s_0 being the specific moist entropy at each grid point and the average specific moist entropy. The usage of moist entropy perturbation $(s - s_0)$, makes equation (2) similar to an eddy flux calculation. In later chapters, when lateral entrainment of moist entropy is discussed, it actually refers to lateral entrainment of moist entropy perturbation. The specific moist entropy is calculated as in *López Carrillo and Raymond* [2005] and *Raymond* [2013], with mixing ratios of liquid

and ice set to zero and r being the mixing ratio of water vapor:

$$s = (C_{pd} + rC_{pv}) \ln(\frac{T}{T_R}) - R_d \ln(\frac{p_d}{p_R}) - rR_v \ln(\frac{p_v}{p_{TP}}) + \frac{L_R r}{T_R} \tag{3}$$

C_{pd} and C_{pv} are specific heat of dry air and water vapor at constant pressure (1005 J $K^{-1}kg^{-1}$ and 1850 J $K^{-1}kg^{-1}$), R_d and R_v are gas constants for dry air and water vapor (287.05 J $K^{-1}kg^{-1}$ and 461.5 J $K^{-1}kg^{-1}$). T_R , p_R and p_{TP} are freezing point of water (273.15 K), reference pressure (1000 hPa) and triple point pressure for water (6.1078 hPa), L_R is the latent heat of condensation (2.5008106 J kg^{-1}). T, p_d and p_v are air temperature (K), pressures of dry air and water vapor (hPa). The average specific moist entropy is calculated from moist entropy per unit mass ($s(x, y, z)$) at all grid points inside the chosen domain:

$$s_0 = \frac{\int\int\int s(x, y, z)\, dx\, dy\, dz}{\int\int\int dx\, dy\, dz} \tag{4}$$

The volume of integration is determined by $4^\circ \times 4^\circ$ mask and the vertical extent of 3D-Var grid used in this analysis (0 to 16 km). The calculation of moist entropy lateral entrainment with perturbations ($s - s_0$) reduces numerical issues that arise when calculating the derivatives. The divergence of moist entropy flux can be separated into two parts:

$$\nabla \cdot (\rho s \mathbf{v}) = \rho \mathbf{v} \cdot \nabla s + s \nabla \cdot (\rho \mathbf{v}) \tag{5}$$

ρ and s are same as before, ∇ and $\mathbf{v}$ are three-dimensional differential operator and wind speed, respectively. The second term on the right side of equation (5) should be zero, following the mass continuity equation, making the divergence of moist entropy flux same as the advection of moist entropy. However, mass continuity is not completely satisfied in our calculations, due to the numerical divergence calculations and the interpolating techniques in 3D-Var analysis. 3D-Var analysis interpolates the data onto regular grid

by balancing between the data from dropsondes and the mass continuity. The vertical velocity is still strongly dependent of horizontal divergence, but it is not perfectly balanced numerically. The resulting mass flux divergence is few orders of magnitude smaller than the other terms in (5), but it is not exactly zero. In our calculations of moist entropy flux divergence, second term on the right side of (5) becomes too big to neglect. In order to decrease the error related to mass continuity deviation, we introduce the subtraction of average entropy into our calculations. This does not change anything if mass continuity is satisfied, but it decreases the magnitude of the term that should be zero. In calculations of lateral entrainment of moist entropy (equation (2)) we are using horizontal divergence, which introduces the artificial term $-s_0\nabla_{\mathbf{h}}\cdot(\rho\mathbf{v_h})$. This term introduces significant changes in vertical profiles at heights where the convergence or divergence is strong. At the surface, the moist entropy advection and convergence become more important relative to mass convergence. Particular situations will be discussed in later chapters. Vertically averaged results are more robust. In the moisture equivalent of equation (5), the second term on the right side is small compared to moisture advection and divergence of moisture flux. Therefore, the moisture lateral entrainment calculation is simpler (equation (1)).

The surface fluxes require sea surface temperatures (SST). We obtain the daily SST data with 0.25° resolution from NOAA's National Centers for Environmental Information [*Reynolds et al.*, 2007]. This product is very useful for bulk surface fluxes, as both spatial and temporal resolution satisfy the needs of our budget calculations. Bulk surface fluxes of moist entropy and moisture are:

$$F_{xs} = C_E\rho v_s(x_s - x_0) \tag{6}$$

The bulk moisture exchange coefficient is $C_E = 0.00118$, as indicated in *Drennan et al.* [2007]. ρ and v_s are the air density and the Earth-relative horizontal wind speed magnitude at the lowest grid level of the 3D-Var analysis. x_s and x_0 are the values of the moist entropy or the mixing ratio of water vapor at the surface and the lowest grid level, respectively. The surface value is the saturated value at the sea surface temperature, while the lowest grid level is taken to be 0 m, since it is the closest to the often used 10 m height.

The radiative cooling entropy loss and irreversible generation of moist entropy are estimated from satellite data, in an effort to estimate all parts of the moist entropy budget. The cloud top temperature from Moderate Resolution Imaging Spectroradiometer (MODIS) instrument on NASA's Aqua and Terra satellites [*Platnick, S., et al.*, 2015] is used for the radiative cooling estimate, which is then used for related entropy loss:

$$F_{rad} = \sigma T_t^3 \tag{7}$$

$-F_{rad}$ is the entropy loss due to radiative cooling, $\sigma = 5.67 \times 10^{-8}$ J s^{-1}m^{-2}K^{-4} is the Stefan-Boltzman constant and T_t is the cloud top temperature.

The irreversible entropy source is estimated from radiative cooling. The relationship is derived from the energy and entropy conservation in radiative-convective equilibrium [*Pauluis and Held*, 2002a; *Warner*, 2005; *Emanuel and Bister*, 1996], with the same amount of energy coming from the surface fluxes and leaving at the top of tropical cyclone, as radiative cooling. Corresponding entropy fluxes are not the same, and the difference is assumed to be due to the irreversible generation of entropy. We use this relation for estimate of irreversible entropy generation in our budget analysis:

$$G = (1 - \frac{\overline{T}_t}{\overline{T}_s})\overline{F}_{rad} \tag{8}$$

G represents the irreversible entropy generation source, $\overline{T}_t$ and $\overline{T}_s$ are the horizontally averaged cloud top and sea surface temperatures, respectively. This estimate is made with the assumption that the irreversible entropy generation does not change significantly from the radiative-convective equilibrium. Since the irreversible entropy generation is small compared to other budget contributors, this assumption does not significantly affect the budget calculations.

The vertical profile for each three-dimensional variable is obtained by horizontal averaging over a chosen domain ($4^\circ \times 4^\circ$ mask). In budget calculations we use horizontally averaged and vertically integrated values. Those will be indicated by square brackets. If the variable has only two dimensions, only the horizontal averaging is done, and that is indicated by overbar. The integrated moist entropy budget equation is:

$$\frac{\partial[\rho s]}{\partial t} = -[\nabla_{\mathbf{h}} \cdot (\rho \mathbf{v}_{\mathbf{h}}(s - s_0))] - \rho w(s - s_0)|_{top} + \overline{F}_{ss} - \overline{F}_{rad} + (1 - \frac{\overline{T}_t}{\overline{T}_s})\overline{F}_{rad} \qquad (9)$$

with $\partial[\rho s]/\partial t$ being total moist entropy tendency, $\rho w(s - s_0)|_{top}$ is vertical flux at the top, $\overline{F}_{ss}$ marks the moist entropy surface flux (equation (6)) and all other parts are described in previous paragraphs. The moisture budget consists of the lateral entrainment, outflow at the top, and the surface fluxes, which results in the rainfall R in the steady state ($\partial[\rho r]/\partial t = 0$):

$$\frac{\partial[\rho r]}{\partial t} + \overline{R} = -[\nabla_{\mathbf{h}} \cdot (\rho \mathbf{v}_{\mathbf{h}} r)] - \rho w r|_{top} + \overline{F}_{rs} \qquad (10)$$

We use the mixing ratio of water vapor (r) as a measure of moisture. Everything except rainfall has the counterpart in the moist entropy budget equation. In both budgets, we made the assumption that the vertical outflow at the top of the storm is small enough to be neglected, which is supported by the results. In our moisture budget results, the total

moisture tendency will only include lateral entrainment and surface fluxes. Note that this calculation of total moisture tendency makes it highly dependable on the rainfall.

3. Case Studies

3.1. Edouard(2014)

In 2014, four HS3 research flights targeted Hurricane Edouard in different stages of the storm's evolution. Edouard's life cycle is described in the Tropical Cyclone Report by *Stewart* [2014]. Prior to the Global Hawk flight on September 11-12, 2014, Edouard had intensified to a tropical storm and was intensifying during the flight. The flight pattern was the lawnmower pattern, with a higher density of drops near Edouard's center. It was followed by a couple of center crossings. There were 60 dropsondes deployed during this flight.

The next flight, on September 14-15, 2014, encompassed a period in which Edouard was at hurricane strength and was undergoing near-rapid intensification. This mission had good dropsonde coverage of the environment by lawnmower pattern and the storm itself by center crossings, which was done with 80 dropsondes.

The third Edouard research flight took place when Hurricane Edouard passed its peak intensity and started decaying, on September 16-17, 2014. The flight pattern consisted of repeated crossings of Edouard's core, with outward coverage extending far enough to be outside the rain bands and convection associated with it. The number of dropsondes in this flight was 87.

The final flight into this system, on September 18-19, 2014, was conducted when Edouard was in a high wind shear area, far north and over colder SST. Therefore, it was decaying and was downgraded to tropical storm status. The upper- and lower-level

centers of vorticity were separated due to the high wind shear. The flight pattern consisted of 50 dropsondes and was similar to the first two Edouard flights, with center crossings being less on target because of the sheared vortex.

The naming convention will be simplified in upcoming sections, with Edouard 1 referring to the first, Edouard 2 to the second research flight, etc. Edouard 1 and 2 are intensifying cases, in tropical storm and hurricane stages; Edouard 3 gives us a look at the hurricane at its peak, but decaying; Edouard 4 is a decaying case. This is an excellent data set for exploring how the moist entropy and moisture budgets change in different stages of a tropical cyclone's life-cycle.

3.2. Gabrielle(2013)

Three research flights were done during Gabrielle's life-cycle [*Avila*, 2013]. The first flight, on August 29-30, 2013, was conducted during the tropical wave stage. The wave was not named yet, but had the designation P25L. The intensity did not change much during this research flight. The spatial coverage was broad, with a lawnmower pattern followed by a center crossing. 72 sondes were deployed, but only the lawnmower drops were used for the 3D-Var analysis.

The second flight, on September 04-05, 2013, caught the system's decay from a tropical depression back to a disturbance. There was another convective system, to the northeast of Gabrielle, that was covered with this research flight, which launched 80 dropsondes. However, we separated the drops from two systems for our analysis. One caveat for this mission was the flight restriction south of Gabrielle, so the domain choice was limited, but still adequate.

The last Gabrielle research flight was done on September 07-08, 2013 when the storm was maintaining its intensity despite high wind shear. It redeveloped a couple of days later. The flight consisted of 2 lawnmower patterns, the first covering the broader environment and the second concentrated more on the storm itself. The dropsondes used in the analysis are the ones closer to Gabrielle's center.

For simplicity, the three described research flights will be referred to as Gabrielle 1, 2 and 3, respectively. Tropical storm Gabrielle is used as an example of non-developing or decaying storm, making all three cases non-intensifying.

4. Results

4.1. Edouard

The analysis of the Edouard cases will be presented in this section. The moist entropy budget results, with all the budget contributors represented by differently colored marks, are shown in Figure 1a. Note that the lines between the dots are used for easier tracking of different budget terms, as well as the differences between consecutive flights. This does not represent interpolated values for days between flights. The time difference between the flights is two days or more, and is too great for such assumption. The same is true for other budget plots. The irreversible generation of entropy is estimated from the radiative cooling. Therefore, the sum of their entropy budget counterparts is negative, as can be seen in (9).

The values of the total, column-integrated, moist entropy tendency, shown in Figure 1c, show the difference between the intensifying and non-intensifying stages. Edouard 1 (Sept 11) and Edouard 2 (Sept 14) are intensifying and have positive values of total moist

entropy tendency, while Edouard 3 (Sept 16) and Edouard 4 (Sept 18) are decaying cases and have negative values of total moist entropy tendency.

Whether the tropical cyclone increases or decreases its moist entropy through the lateral exchange with the environment (red dots in Figure 1a), depends on the inflow close to the surface, as well as the entropy flow at middle and higher levels. This is further examined by vertical profiles of lateral entropy import, shown in Figure 2a-d.

Edouard 1 and 2 cases show strong moist entropy perturbation import through the lowest 1 km, unlike Edouard 3 and 4. The latter two cases even exhibit export above 0.5 km. In the typical vertical profile, moist entropy has a local maximum at lower levels, making those levels the best source of moist entropy through the lateral exchange. So, the existence of a strong low-level import makes further development more likely. Vertical profiles of vertical mass flux, shown in Figure 2e-h, have strong positive gradient close to the surface, indicating the existence of a low-level convergence in all 4 Edouard cases. The gradients grow with time, with the last Edouard case experiencing the strongest low-level convergence. As was noted in the Methods section, the calculation of lateral entrainment of moist entropy perturbation (equation (2)) reduces the sensitivity to the mass convergence. It does so most prominently close to the surface. As it can be observed from Figure 2, the decaying cases have stronger mass convergence, but weaker entropy perturbation import at lowest 1 km.

Figures 1b and d show the individual sources of moisture and the incomplete moisture budget, for all Edouard flights. Note that our total moisture tendency includes only lateral entrainment and surface fluxes, not the rainfall. There is no noticeable difference in moisture tendencies between Edouard's intensifying and decaying cases. Edouard's

moisture surface fluxes follow similar pattern as the moist entropy surface fluxes, with Edouard 4 having the lowest values. However, the lateral import of moisture is much stronger than surface fluxes in all 4 cases, making them the strongest influence on the total moisture tendency. Furthermore, the lateral entrainment of moisture is mostly influenced by the convergence near the surface (Figure 2a-d). Edouard 2 and 3 have similar values of near-surface import of moisture, but above 1 km Edouard imports more during intensification. The strongest convergence of moisture happens during Edouard's decay, but other factors inhibit the development, which will be discussed later.

The first Edouard mission (Edouard 1, Sept 11-12, 2014), which happened during the tropical storm and intensifying stage, has the strongest moist entropy import at low levels, with weaker export above, caused by almost constant vertical mass flux throughout most of the troposphere (Figure 2a and e). Column-integrated lateral entrainment of moist entropy is close to zero (first red dot in Figure 1a). It is then up to the surface fluxes to increase the moist entropy.

The second mission occurred while Hurricane Edouard (Edouard 2) was intensifying, on Sept 14-15, 2014. Even though the overall lateral export of moist entropy was strong, the surface flux was even stronger, increasing the moist entropy in Hurricane Edouard. Note that this situation is different than tropical storm or depression stages. Here, the tropical cyclone is well organized and it has a lot of moisture and energy, as well as strong surface fluxes, so the lateral moist entropy export can be higher and still be favorable for intensification.

Edouard 3 (Sept 16-17, 2014) represents the first decaying case, after reaching peak intensity. Its vertical profiles are shown in Figure 2c,g,k. The moist entropy export

happens throughout the troposphere, with the exception of few shallow layers. This is the reason Edouard 3 has the highest loss of entropy due to lateral exchange (minimum in red dots in Figure 1a). In this case, the surface fluxes are a bit lower than in Edouard 2, and not strong enough to compensate the loss through the lateral export. The entropy export is occurring even close to the surface, where mass convergence is strong. This could be the consequence of dry air intrusion coming from northeast and south, which happens below 1 km (not shown). The near-surface layers advecting drier air seem to have a bigger effect on moist entropy than on moisture lateral entrainment.

Edouard 4 is an interesting decaying case, because of the strong moist entropy import in mid-levels (5 - 9 km), as seen in Figure 2d. This is caused by the divergence at those levels, which is supported by the negative gradient in vertical mass flux (Figure 2h). Here, the entropy increase does not come from import of higher values of moist entropy, but from the export of mid-level lower values. Even though the mid-level divergence introduces a positive moist entropy perturbation in the tropical cyclone, it also destroys the vortex. Figure 3 shows the vorticity tendency due to stretching and total vorticity tendency at 6 km. Divergence affects the stretching part of vorticity tendency, which decreases the vorticity over entire domain. The maximum reduction happens around the vortex center. The negative signal is so strong, that it is still visible in total vorticity tendency. Tilting of vorticity introduced a dipole, with increase of vorticity southwest from the vortex, but the decrease around the vortex is still there. This divergence is related to strong environmental shear, which creates the vortex tilt [*Jones*, 1995], opening up the inner structure of Edouard to outside air. Since the circulation centers at different heights are not aligned anymore, the protection from environmental air intrusion, as

described in *Dunkerton et al.* [2009] and *Raymond and López Carrillo* [2011], does not exist. Additionally, *Zawislak et al.* [2016] showed that strong vertical wind shear dried upshear parts of Edouard through the shear-induced subsidence. Another interesting feature of this case is the strong moisture inflow, stronger than other Edouard cases, extending from surface to above 1km (Figure 2l). This, in conjunction with entropy export at same levels, is a sign of convergence of cool and moist air.

At this point, during Sept 18-19, 2014 mission, Edouard had a lot of moisture coming in from low levels, but at low temperatures. This is the consequence of lower sea surface temperatures (SST) along the Edouard's path. The storm reached 40N and the SST around Edouard was between 20 and 26C, according to NOAA's daily SST data. On the other hand, the mid-level divergence was very strong, exporting low moist entropy and destroying the mid-level vortex. The likely cause for this kind of divergence is strong vertical wind shear, that became the important factor in this part of Edouard's life-cycle.

4.2. Gabrielle

Unlike Edouard, Gabrielle was not well organized during any of the three Global Hawk missions, reaching only the tropical depression strength. Also, it was not intensifying during any of the flights, and was decaying during the second flight.

The total moist entropy tendency is negative for all three Gabrielle missions, and more negative than the two Edouard decaying cases (Figures 1c and 4c). Radiative cooling plays a big role (green dots in Figure 4a), having higher or comparable effect as lateral entrainment and surface fluxes. The reason for such strong radiative cooling is smaller cloud-covered area and less convective activity than encountered in Edouard missions. Despite negative moist entropy tendency, Gabrielle 1 and 3 did not decay, making them

the null cases. The real decaying case is Gabrielle 2, with strongest net entropy loss. When compared to other two Gabrielle cases, Gabrielle 2 is losing less moist entropy through radiative cooling, but exports much more through lateral exchange with the environment. This loss of moist entropy is strong enough to overcome the gain from the surface fluxes.

The lateral moisture entrainment and the moisture surface fluxes in Gabrielle are much smaller than in Edouard (Figures 1b and 4b). This is expected considering the much lower intensity of Gabrielle. However, during Gabrielle's decay (Gabrielle 2, Sept 04-05, 2013), the moisture is laterally exported between 1 and 4 km altitude (Figure 5h). In this case, the lateral export of moisture is stronger than surface fluxes, causing overall drying of the tropical cyclone (negative value in Figure 4d).

Similar to Edouard analysis, we will present the vertical profiles for Gabrielle missions. All vertical profiles will be shown on the same scale as corresponding Edouard figures, for easier comparison. Figure 5a-c shows the vertical profiles of lateral moist entropy entrainment for three Gabrielle cases. The magnitudes of lateral exchange are smaller than in Edouard. Also, the surface moist entropy perturbation import is small in all three Gabrielle cases, with Gabrielle 2 having the minimum. However, Gabrielle 2 has maximum amplitudes above, strongest import around 3 km and export around 6 km. The strong entropy export around 6 km is related to the inflow of very dry air from the north and northwest (Figure 7).

The vertical mass flux and lateral moisture import (Figure 5d-i) have smaller magnitudes than in Edouard cases. The relative magnitudes of moist entropy and moisture import in three Gabrielle cases near the surface are the same, with Gabrielle 1 having the strongest, and Gabrielle 2 the weakest import. The Gabrielle 2 vertical mass flux vertical profile

shows subsidence between 2 and 7 km. Our analysis indicates that this is mostly coming from the northern part of the domain.

The moist entropy import at 3 km during the Sept 04-05, 2013 (Gabrielle 2) research flight is especially interesting when examined in conjunction with vertical profile of lateral moisture entrainment (Figure 5b and h). Even though the moist entropy is imported, the moisture is being exported. This is partially due to suppressed divergence effect on entropy entrainment, as discussed in Methods section. Another possible reason for the mentioned discrepancy is the warm and dry air. As it can be seen from horizontal cuts at 2 km in Figure 6, there is a warm and dry anomaly occurring in the southeastern corner of Gabrielle. This could be the result of a strong convective activity that happened before the measurement, leaving the dry and warm anomaly above the cool and saturated surface layer in its wake [*Zipser*, 1977; *Houze*, 1977]. *Zipser* [1977] described the existence of two very distinct layers behind a tropical squall line, created by two kinds of downdrafts. The lowest few hundred meters are cool and saturated, above that is a layer of drier air, that can exhibit warmer temperatures than its surroundings. Zipser hypothesized that convective-scale saturated downdrafts created a shallow surface layer of cool, near-saturated air, while mesoscale unsaturated downdrafts created the layer of unsaturated air above. Satellite images taken during the mission indicate some convective activity in the vicinity of the warm and dry anomaly in the measurements. It is possible that our vertical profiles are showing something similar to the warm, dry layer following a squall line passage described in *Zipser* [1977].

During the second research flight (Sept 04-05, 2013), tropical depression Gabrielle was ingesting dry air at multiple levels, as indicated by vertical profiles of moist entropy and

moisture entrainment, while having very weak import of moisture close to the surface. This dry air intrusion at multiple levels was mostly the result of dry environmental air, with the addition of localized dry air anomaly around 2 km height, which was transported further into the storm (Figure 6). This anomaly was possibly left behind by Gabrielle's convective activity in the south-east corner. Therefore, it is a possible contributor, in addition to the dry environmental air, to its decay on September 04-05, 2013.

4.3. Larger dataset

In order for our dataset to be more robust, we expand our analysis to other intensifying and non-intensifying tropical cyclones. We use the data from other research flights during the HS3 campaign, as well as dropsonde data from the Tropical Cyclone Structure (TCS08) project [*Elsberry and Harr*, 2008] and NOAA Hurricane Research Division's (HRD) aircraft missions[*NOAA/AOML/Hurricane Research Division*, 2010]. All missions are described in Table 1. If the target system decays or stays at the same intensity during the research flight, then it is designated as non-intensifying. The intensifying cases include all missions that observed the intensification. In total, we have 11 non-intensifying and 12 intensifying cases, in different stages of their life-cycle. Additionally, 10 are a tropical storm or a hurricane, while other 13 are a tropical depression, a disturbance or a wave. The research flights from Edouard (2014) and Gabrielle (2013) are included.

Most of the conclusions derived from Edouard and Gabrielle data hold for this bigger dataset. The moist entropy tendency is positive for intensifying and negative for non-intensifying cases (Figure 8bottom). The radiative cooling is weaker during intensification (Figure 8top). The partial moisture budget is better related to the observed tropical cyclone intensity than the development potential, with tropical storms and hurri-

canes having higher values than tropical depressions and disturbances (Figure 9bottom). In the moisture budget, the lateral entrainment plays a more important role than the surface fluxes (Figure 9top). The dominance of moisture lateral entrainment in moisture budget occurring in this dropsonde dataset confirms the results from the numerical models [*Trenberth et al.*, 2007] and the global analysis [*Kilroy et al.*, 2016].

5. Conclusions

The primary goal of this paper is to establish the connection between the moist entropy budget and tropical cyclone development, by analyzing the satellite and HS3 dropsonde data from Hurricane Edouard (2014) and Tropical Storm Gabrielle (2013). The first two Edouard missions are examples of intensifying cases, while the other two Edouard and all three Gabrielle missions are considered non-intensifying. The total moist entropy budget indicates moist entropy increase for intensifying cases, and decrease for non-intensifying cases (Figures 1c and 4c). Our analysis supports the hypothesis that overall moist entropy increase relates to tropical cyclone intensification. This could be considered as a necessary, but not sufficient condition for intensification. Our moisture tendency calculations show better differentiation between stronger and weaker tropical cyclone (higher values for Edouard, lower for Gabrielle, Figures 1d and 4d) than between intensifying and non-intensifying cases. This is expected due to our calculation of total moisture tendency and its connection to the rainfall.

The expanded dataset confirms the moist entropy budget's close relationship with the tropical cyclone evolution (intensification or non-intensification), and the moisture tendency's relation to the current state of the tropical cyclone (Figures 8 and 9). Also, the moisture tendency depends more on the moisture lateral entrainment than the moisture

surface fluxes, for both intensifying and non-intensifying cases. These patterns in the moist entropy and moisture budgets are expected from examining previous theories and analyses, but this paper provides the observational confirmation from very detailed in-situ data.

The moist entropy budget is calculated from four contributors: surface fluxes, lateral entrainment, radiative cooling and irreversible generation of moist entropy. Radiative cooling and irreversible generation estimates are connected in our analysis, contributing negatively to the moist entropy tendency. From the work done on relating the gross moist stability to convection [*Neelin and Held*, 1987; *Raymond et al.*, 2007; *Raymond and Sessions*, 2007], it can be assumed that the weak lateral detrainment relates to strong convective activity, which supports tropical cyclone development. That can be assumed only in earlier stages of tropical cyclone's life-cycle. Before the hurricane stage, surface fluxes and irreversible generation of entropy are weaker and radiative cooling is stronger, which makes the storm more dependent on lateral entrainment as the source of moist entropy and moisture. In the hurricane stage of Edouard's evolution, the storm exhibits relatively strong lateral detrainment of moist entropy, leaving the surface fluxes as the main source. Once the surface fluxes diminish, the moist entropy in Edouard decreases, and we hypothesize this is one of the causes for the decay. A similar situation occurs in Gabrielle's decay, with the additional influence of strong radiative cooling. Overall, the sign of the total moist entropy tendency depends on the ability of the surface fluxes to overcome losses due to the radiative cooling and lateral entrainment. The moist entropy budget as the possible intensification indicator is practically useful because all the im-

portant information comes from outside the inner core, making the needed data easier to obtain.

The last Edouard case was different, with column-integrated lateral entrainment being close to zero. The main reason for this discrepancy was at the height where strongest lateral entrainment occurs. During Edouard 4, most of the moist entropy increase originated at mid-levels (4 - 8 km). This increase was due to the export of low moist entropy out of the system, rather than the import of higher values. The same divergence that caused the low entropy export, could also destroy the vortex, leading to the decay. The strong divergence, evident from the shape of the vertical mass flux profile, was probably caused by increasing environmental vertical wind shear. Vertical wind shear became an important factor in Edouard's development by the time of the last HS3 mission, bringing asymmetries in moisture, vertical velocity and precipitation. At the same time, Edouard was importing significant amount of moisture. However, the entropy was weakly imported and even exported between surface and 1 km height. This was caused by the convergence of moist, but cold air, which was likely related to low sea surface temperatures that Edouard encountered. Low sea surface temperatures also decreased the surface fluxes, reducing Edouard's resilience to increasing environmental shear.

Gabrielle's decay during the September 04-05, 2013 research flight was probably caused by a dry environment, with additional drying induced by the warm and dry anomaly around 2 km. It is possible that this anomaly was a remnant of previous convective activity.

The strength of this paper is in the observational point of view of the thermodynamic budgets' relations with the tropical cyclone intensification or decay. However, this explains

only some of the processes happening during the tropical cyclone evolution. In the future, we will examine the complicated interplay between the dynamic and thermodynamic variables, as well as the importance of deep convection and inner core processes.

Acknowledgments. This work was supported by NASA grant NNX12AJ80G and U.S. National Science Fundation grant ATM-1342001. The dropsonde data used for this paper was collected by the HS3, TCS08 and NOAA/AOML/HRD teams, prepared by UCAR/NCAR-EOL and we would like to thank them for their efforts. We would like to thank Roger Smith, Steve Garner and one anonymous reviewer for their useful comments that improved this manuscript. The dropsonde and satellite data sources are listed in references. 3D-Var analysis results are available at http://kestrel.nmt.edu/ raymond/data/index.xhtml (under HS3analyses). Other data and scripts are available upon request, by contacting the first author at ana.juracic@gmail.com.

References

Avila, L. A. (2013), Tropical Cyclone Report: Tropical Storm Gabrielle 4-13 September 2013, National Hurricane Center, Miami, FL, Available online at http://www.nhc.noaa.gov/data/tcr/AL072013_Gabrielle.pdf.

Drennan, W. M., J. A. Zhang, J. R. French, C. McCormick, and P. G. Black (2007), Turbulent fluxes in the hurricane boundary layer. Part II: Latent heat flux, *J. Atmos. Sci.*, *64*, 1103–1115, doi:10.1175/JAS3889.1.

Dunkerton, T. J., M. T. Montgomery, and Z. Wang (2009), Tropical cyclogenesis in a tropical wave critical layer: Easterly waves, *Atmos. Chem. Phys.*, *9*, 5587–5646.

Elsberry, R., and P. A. Harr (2008), Tropical cyclone structure (TCS08) field experiment science basis, observational platforms, and strategy, *Asia Pac. J Atmos. Sci.*, *44*, 209–231.

Emanuel, K. A. (1999), Thermodynamic control of hurricane intensity, *Nature*, *401*, 665–669, doi:10.1038/44326.

Emanuel, K. A., and M. Bister (1996), Moist convective velocities and buoyancy scales, *J. Atmos. Sci.*, *53*, 3276–3285.

Emanuel, K. A., C. DesAutels, C. Holloway, and R. Korty (2004), Environmental control of tropical cyclone intensity, *J. Atmos. Sci.*, *61*, 843–858.

Gjorgjievska, S., and D. J. Raymond (2014), Interaction between dynamics and thermodynamics during tropical cyclogenesis, *Atmos. Chem. Phys.*, *14*, 3065–3082, doi:10.5194/acp-14-3065-2014.

Hock, T., K. Young, and H. Voernel (2016), Hurricane and Severe Storm Sentinel (HS3) Global Hawk Advanced Vertical Atmo-

588 spheric Profiling System (AVAPS) Dropsonde System [2013, 2014], doi:
589 http://dx.doi.org/10.5067/HS3/AVAPS/DROPSONDE/DATA201, Dataset avail-
590 able online [https://hs3.nsstc.nasa.gov/pub/hs3/AVAPS/] from the NASA Global
591 Hydrology Resource Center DAAC, Huntsville, Alabama, U.S.A.

592 Houze, R. A., Jr. (1977), Structue and dynamics of a tropical squall line system, *Mon.*
593 *Wea. Rev.*, *105*, 1540–1567.

594 Inoue, K., and L. Back (2015), Column-integrated moist static energy analysis on various
595 time scales during TOGA COARE, *J. Atmos. Sci.*, *72*, 1856–1871, doi:10.1175/JAS-D-
596 14-0249.1.

597 Jones, S. C. (1995), The evolution of vortices in vertical shear: 1. Initially barotropic
598 vortices, *Quart. J. Roy. Meteor. Soc.*, *121*, 821–851, doi:10.1002/qj.49712152406.

599 Kilroy, G., R. K. Smith, M. T. Montgomery, B. Lynch, and C. Earl-Spurr (2016), A case
600 study of a monsoon low that formed over the sea and intensified over land as seen in
601 the ECMWF analyses, *Quart. J. Roy. Meteor. Soc.*, doi:10.1002/qj.2814.

602 López Carrillo, C., and D. J. Raymond (2005), Moisture tendency equations in a tropical
603 atmosphere, *J. Atmos. Sci.*, *62*, 1601–1613, doi:10.1175/JAS3424.1.

604 López Carrillo, C., and D. J. Raymond (2011), Retrieval of three-dimensional wind fields
605 from Doppler radar data using an efficient two-step approach, *Atmos. Meas. Tech.*
606 *Discuss.*, *4*, 2717–2733, doi:10.5194/amt-4-2717-2011.

607 Masunaga, H., and T. S. L'Ecuyer (2014), A mechanism of tropical convection inferred
608 from observed variability in the moist static energy budget, *J. Atmos. Sci.*, *71*, 3747–
609 3766, doi:10.1175/JAS-D-14-0015.1.

Neelin, J. D., and I. M. Held (1987), Modeling tropical convergence based on the moist static energy budget, *Mon. Wea. Rev.*, *115*, 3–12.

NOAA/AOML/Hurricane Research Division (2010), Hurricane Data, 2010 Hurricane Season, Dataset available online [http://www.aoml.noaa.gov/hrd/data_sub/hurr2010.html] from the Hurricane Research Division, Miami, FL.

Pauluis, O. (2011), Water vapor and mechanical work: A comparison of Carnot and steam cycles, *J. Atmos. Sci.*, *68*, 91–102, doi:10.1175/2010JAS3530.1.

Pauluis, O., and I. M. Held (2002a), Entropy budget of an atmosphere in radiative-convective equilibrium. Part I: Maximum work and frictional dissipation, *J. Atmos. Sci.*, *59*, 125–139.

Pauluis, O., and I. M. Held (2002b), Entropy budget of an atmosphere in radiative-convective equilibrium. Part II: Latent heat transport and moist processes, *J. Atmos. Sci.*, *59*, 140–149.

Platnick, S., et al. (2015), MODIS Atmosphere L3 Daily Product, NASA MODIS Adaptive Processing System, Goddard Space Flight Center, USA, URL http://dx.doi.org/10.5067/MODIS/MOD08_D3.006.

Raymond, D. J. (2013), Sources and sinks of entropy in the atmosphere, *J. Adv. Model Earth Syst.*, *5*, 755–763, doi:10.1002/jame.20050.

Raymond, D. J., and C. López Carrillo (2011), Vorticity budget of typhoon Nuri, *Atmos. Chem. Phys.*, *11*, 147–163, doi:10.5194/acp-11-147-2011.

Raymond, D. J., and S. L. Sessions (2007), Evolution of convection during tropical cyclogenesis, *Geophys. Res. Lett.*, *34*, L06811, doi:10.1029/2006GL028607.

Raymond, D. J., S. L. Sessions, and Ž. Fuchs (2007), A theory for the spinup of tropical depressions, *Quart. J. Roy. Meteor. Soc.*, *133*, 1743–1754, doi:10.1002/gj.125.

Raymond, D. J., S. L. Sessions, and C. López Carrillo (2011), Thermodynamics of tropical cyclogenesis in the northwest Pacific, *J. Geophys. Res.*, *116*, D18101, doi: 10.1029/2011JD015624.

Raymond, D. J., S. Gjorgjievska, S. L. Sessions, and Ž. Fuchs (2014), Tropical cyclogenesis and mid-level vorticity, *Aus. Met. and Ocean J.*, *64*, 11–25.

Reynolds, R. W., T. M. Smith, C. Liu, D. B. Chelton, K. S. Casey, and M. G. Schlax (2007), Daily high-resolution blended analyses for sea surface temperature, *J. Climate*, *20*, 5473–5496, doi:10.1175/2007JCLI1824.1.

Sessions, S. L., S. Sugaya, D. J. Raymond, and A. H. Sobel (2010), Multiple equilibria in a cloud-resolving model using the weak temperature gradient approximation, *J. Geophys. Res.*, *115*, D12110, doi:10.1029/2009JD013376.

Stewart, S. R. (2014), Tropical Cyclone Report: Hurricane Edouard 11-19 September 2014, National Hurricane Center, Miami, FL, Available online at http://www.nhc.noaa.gov/data/tcr/AL062014_Edouard.pdf.

Trenberth, K. E., C. A. Davis, and J. Fasullo (2007), Water and energy budgets of hurricanes: Case studies of Ivan and Katrina, *J. Geophys. Res.*, *112*, D23,106, doi: 10.1029/2006JD008303.

UCAR/NCAR - Earth Observing Laboratory (1993-present), NCAR Airborne Vertical Atmospheric Profiling System (AVAPS), doi:http://dx.doi.org/10.5065/D66W9848.

Warner, C. (2005), Entropy sources in equilibrium conditions over a tropical ocean, *J. Atmos. Sci.*, *62*, 1588–1600, doi:10.1175/JAS3422.1.

Young, K., J. Wang, T. Hock, D. Lauritsen, and C. Martin (2013), HS3 2013 quality controlled Global Hawk dropsonde data set.

Zawislak, J., H. Jiang, G. R. Alvey, E. J. Zipser, R. F. Rogers, J. A. Zhang, and S. N. Stevenson (2016), Observations of the structure and evolution of Hurricane Edouard (2014) during intensity change. Part I: Relationship between the thermodynamic structure and precipitation, *MWR*, doi:http://dx.doi.org/10.1175/MWR-D-16-0018.1.

Zipser, E. J. (1977), Mesoscale and convective-scale downdrafts as distinct components of squall-line structure, *Mon. Wea. Rev.*, *105*, 1568–1589.

Table 1. Parameters for all missions used for the larger dataset[a]

Mission	Date	Location	Development	Stage	Source
Edouard1 (E1)	11-12 Sept 2014	42.5W, 18N	Intensify	TS	HS3
Edouard2 (E2)	14-15 Sept 2014	53W, 25.5N	Intensify	Hurr	HS3
Edouard3 (E3)	16-17 Sept 2014	57W, 33N	Decay	Hurr	HS3
Edouard4 (E4)	18-19 Sept 2014	40W, 39.5N	Decay	Hurr-TS	HS3
Cristobal (C1)	26-27 Aug 2014	71.5W, 30N	Intensify	Hurr	HS3
I90L (I1)	05-06 Sept 2014	28W, 15N	Non-develop	TW	HS3
Gabrielle1 (G1)	29-30 Aug 2013	46W, 15N	Non-develop	TW	HS3
Gabrielle2 (G2)	04-05 Sept 2013	66W, 17.5N	Decay	TD-TW	HS3
Gabrielle3 (G3)	07-08 Sept 2013	68W, 23N	Non-develop	TW	HS3
Humberto (H1)	16-17 Sept 2013	43W, 27.5N	Decay	TS	HS3
I95L (I2)	19-20 Sept 2013	95W, 21N	Non-develop	TW	HS3
Alex1 (A1)	28-29 June 2010	91.5W, 20.5N	Intensify	TS	HRD
Alex2 (A2)	29-30 June 2010	94.5W, 22.5N	Intensify	TS-Hurr	HRD
Karl1 (K1)	12-13 Sept 2010	73W, 16.5N	Intensify	TW	HRD
Karl2 (K2)	13 Sept 2010	79W, 17.5N	Intensify	TW	HRD
Karl3 (K3)	14 Sept 2010	84.5W, 18.5N	Intensify	TS	HRD
Karl4 (K4)	16 Sept 2010	94W, 20N	Intensify	Hurr	HRD
Matthew (M1)	23 Sept 2010	77W, 14N	Intensify	Hurr	HRD
Nuri1 (N1)	15-16 Aug 2008	147E, 14N	Intensify	TW	TCS08
Nuri2 (N2)	16-17 Aug 2008	140E, 15N	Intensify	TD	TCS08
TCS025-1 (T1)	27-28 Aug 2008	152E, 18N	Non-develop	TW	TCS08
TCS030 (T2)	01-02 Sept 2008	143E, 12N	Non-develop	TW	TCS08
Hagupit2 (H2)	14 Sept 2008	147.5E, 18N	Non-develop	TW	TCS08

[a] Position is the center of vorticity at 2 km, and it represents the center of horizontal domain ($4^\circ \times 4^\circ$ mask). Decaying and non-developing cases are classified as non-intensifying. The tropical cyclone stages are: TW - tropical wave, TD tropical depression, TS-tropical storm, Hurr-Hurricane. TW and TD are classified as weak, TS and Hurr as strong systems.

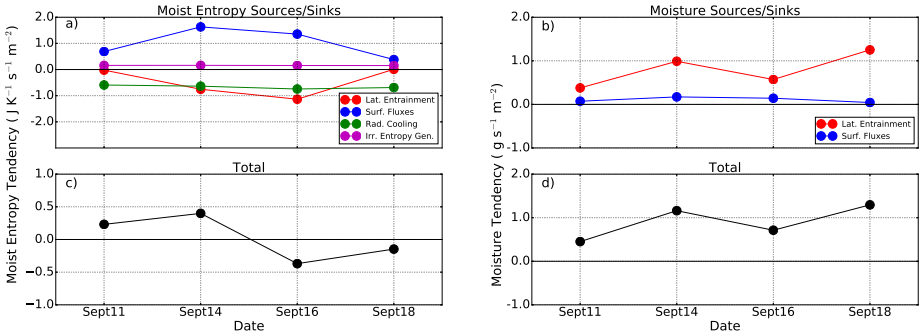

Figure 1. The moist entropy (left) and moisture budgets (right) of Hurricane Edouard during HS3 missions. (a) Moist entropy budget contributions: lateral entrainment of moist entropy (red), surface fluxes (blue), radiative cooling (green), irreversible entropy generation (magenta). (b) Moisture budget contributors: lateral import of moisture (red) and moisture surface fluxes (blue). (c) Total moist entropy tendency (black dots). (d) Total moisture tendency = lateral entrainment + surface fluxes. The lines between dots are used to keep track of difference between results in successive flights, and are not representative of the trend. The horizontal distance between dots is the same for all cases and not representative of time between flights. Naming convention is as follows: Sept11 is Edouard 1, Sept14 is Edouard 2, Sept16 Edouard 3, and Sept18 Edouard 4.

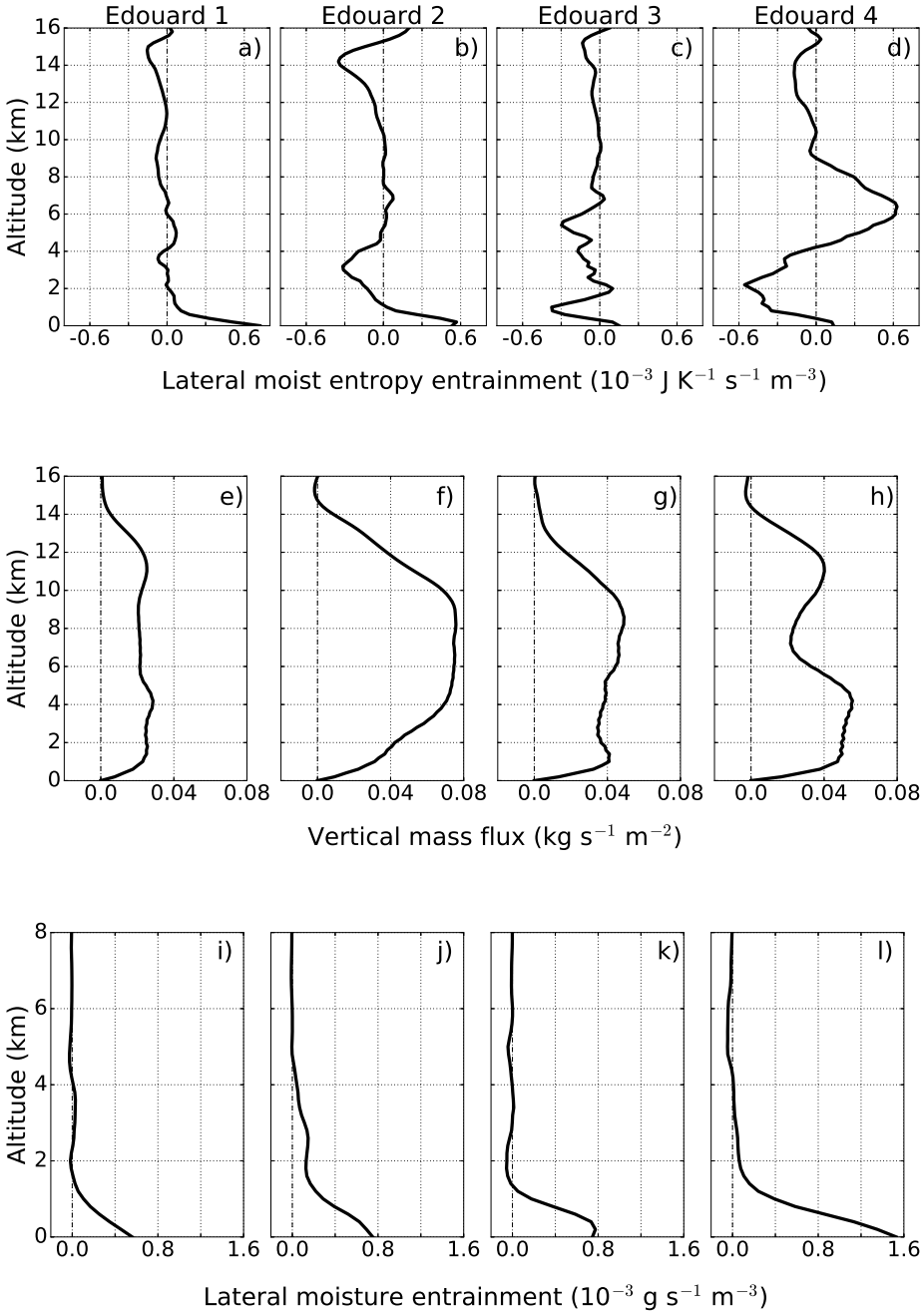

Figure 2. Vertical profiles of lateral entrainment of moist entropy (top), vertical mass flux (middle) and lateral entrainment of moisture (bottom), for 4 Edouard missions. The vertical extent of bottom plot is just up to 8 km, because the moisture import is zero above that. Vertical profiles from Edouard 1 are first on the left, followed by Edouard 2, Edouard 3 and Edouard 4.

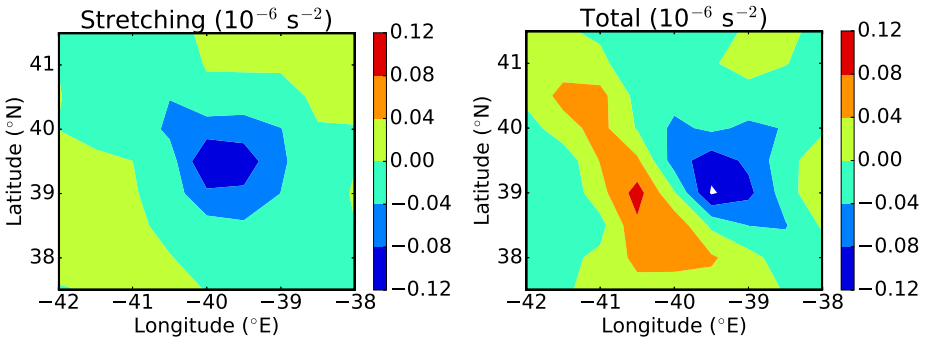

Figure 3. Vorticity tendency for Edouard 4 mission (September 18-19, 2014), at 6 km. Vorticity tendency due to stretching (10^{-6}s^{-2}, left) and total vorticity tendency (10^{-6}s^{-2}, right).

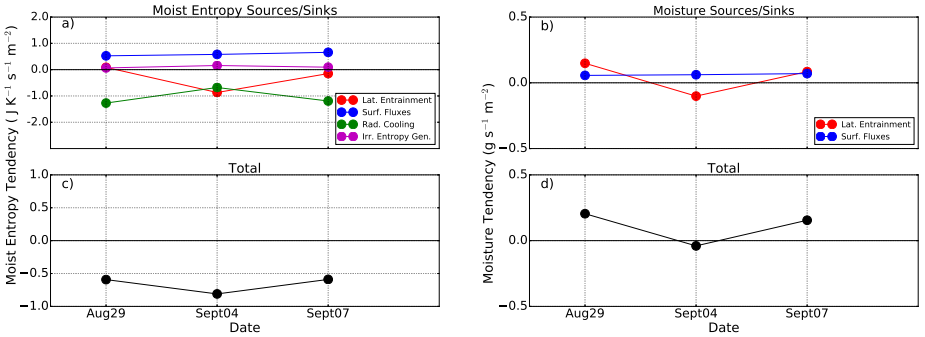

Figure 4. Same as Figure 1, but for Gabrielle. Moisture tendencies have different scale than Edouard cases. Naming convention: Aug29 is Gabrielle 1, Sept04 is Gabrielle 2, and Sept07 is Gabrielle 3.

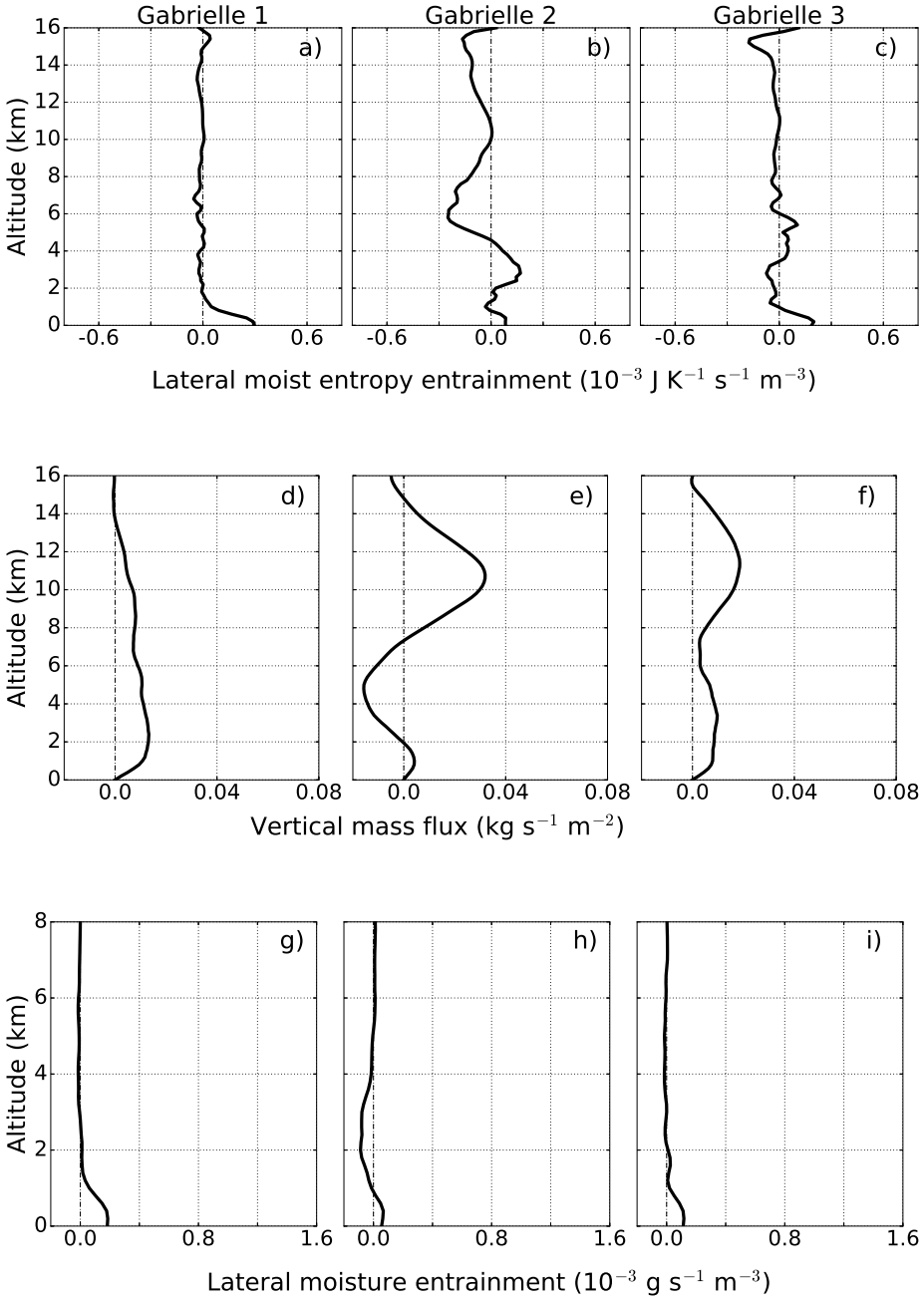

Figure 5. Same as Figure 2, for 3 Gabrielle missions. Gabrielle 1 is far left, followed by Gabrielle 2 and Gabrielle 3. The horizontal and vertical axis limits match ones in respective Edouard plots.

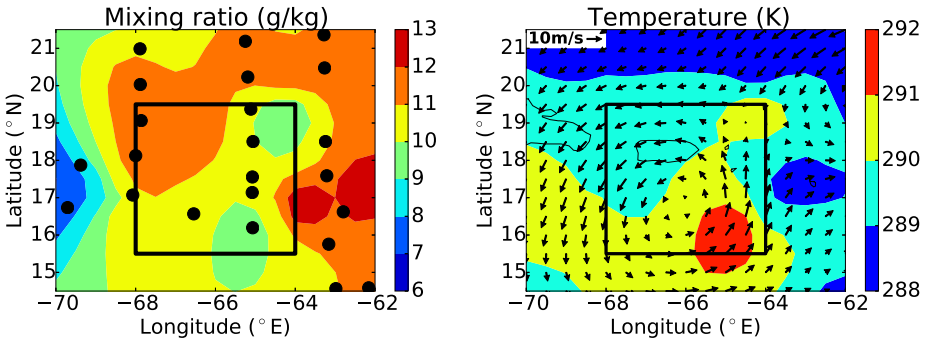

Figure 6. Mixing ratio of water vapor (g/kg, contour plot, left), air temperature (K, contour plot, right) and wind speeds (arrows, right) at 2km, dropsonde positions (black dots), and limits of the domain (black box), for Gabrielle 2 mission (September 04-05, 2013 research flight). Wind speed is storm-relative.

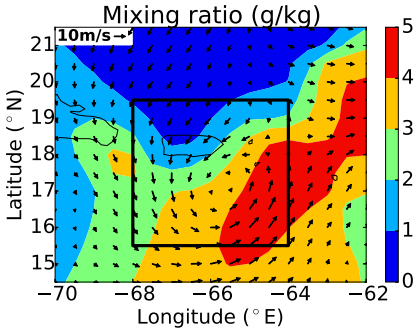

Figure 7. Mixing ratio of water vapor (g/kg) and storm-relative wind speed (arrows) at 6 km, for Gabrielle 2 mission.

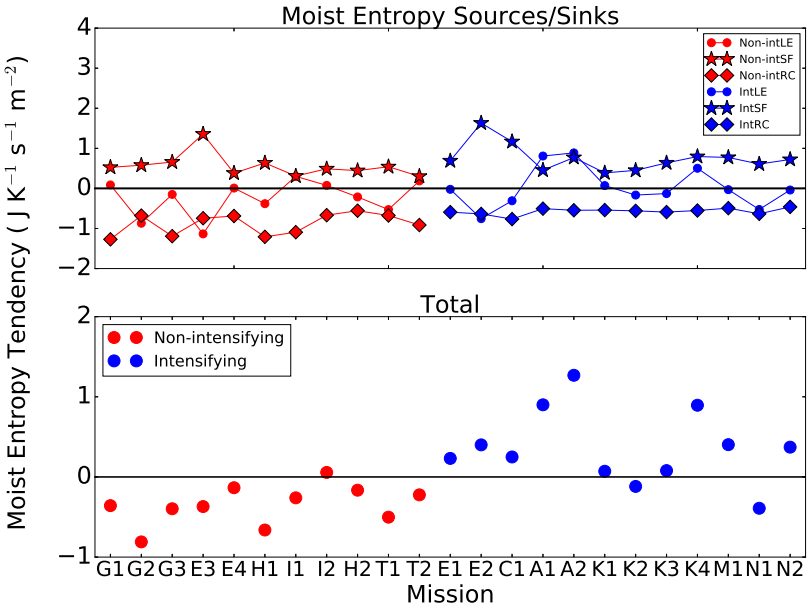

Figure 8. Moist entropy budget for larger dataset (including Edouard and Gabrielle). Top: Moist entropy tendencies due to surface fluxes (stars), lateral entrainment (circles) and loss due radiative cooling (diamonds), for all non-intensifying (red) and intensifying cases (blue). Bottom: Total moist entropy tendency for all non-intensifying (red) and intensifying cases (blue). As in previous sections, the lines between the points are for easier recognition, and do not represent the trend. The mission notation is explained in Table 1.

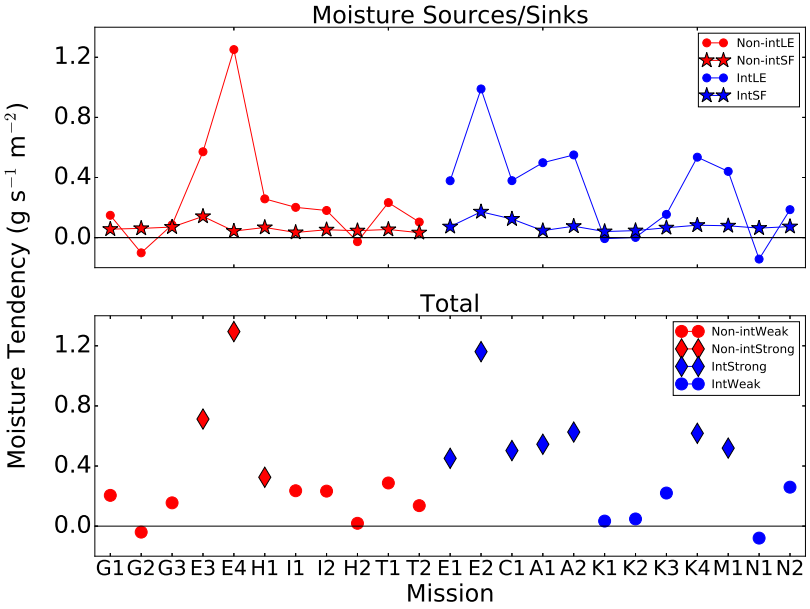

Figure 9. Partial moisture budget for larger dataset. Top: Moisture tendencies due to surface fluxes (stars) and lateral entrainment (circles), for all non-intensifying (red) and intensifying cases (blue). Bottom: Total moisture tendency due to surface fluxes and lateral entrainment, for all non-intensifying (red) and intensifying cases (blue). Tropical storms and hurricanes are diamonds, tropical depressions and disturbances are circles.